Nanoparticulate ZrNi: In-situ Disproportionation Effectively Enhances Hydrogen Cycling of MgH_2

Lingchao Zhang[1], Xin Zhang[1,2], Wenxuan Zhang[1], Zhenguo Huang[3], Fang Fang[4*], Juan Li[5], Limei Yang[3], Changdong Gu[1], Wenping Sun[1], Mingxia Gao[1], Hongge Pan[1,6*], Yongfeng Liu[1,6*]

[1]State Key Laboratory of Silicon and Advanced Semiconductor Materials, Key Laboratory of Advanced Materials and Applications for Batteries of Zhejiang Province and School of Materials Science and Engineering, Zhejiang University, Hangzhou 310058, China.

[2]Taizhou Institute of Zhejiang University, Taizhou 318000, China.

[3]School of Civil & Environmental Engineering, University of Technology Sydney, 81 Broadway, Ultimo, NSW, 2007, Australia.

[4]Department of Materials Science, Fudan University, Shanghai, 200433 China.

[5]College of Materials Science and Engineering, Zhejiang University of Technology, Hangzhou, 310014, China

[6]Institute of Science and Technology for New Energy, Xi'an Technological University, Xi'an, 710021, China.

*Corresponding Author

E-mail: mselyf@zju.edu.cn (Y.F.L.), f_fang@fudan.edu.cn (F.F.), hgpan@zju.edu.cn (H.G.P.)

ABSTRACT: High thermal stability and sluggish absorption/desorption kinetics are still important limitations for using magnesium hydride (MgH_2) as a solid-state hydrogen storage medium. One of the most effective solutions in improving hydrogen storage properties of MgH_2 is to introduce a suitable catalyst. Herein, a novel nanoparticulate ZrNi with 10-60 nm in size was successfully prepared by co-precipitation followed by molten-salt reduction process. The 7 wt.% nano-ZrNi-catalyzed MgH_2 composite desorbs 6.1 wt.% of hydrogen starting from ~178 °C after activation, lowered by 99 ºC relative to the pristine MgH_2 (~277 ºC). The dehydrided sample rapidly absorb ~5.5 wt.% H_2 when operating at 150 °C for 8 min. The remarkably improved hydrogen storage properties are reasonably ascribed to the *in situ* formation of ZrH_2, $ZrNi_2$ and Mg_2NiH_4 caused by the disproportionation reaction of nano-ZrNi during the first de-/hydrogenation cycle. These catalytic active species are uniformly dispersed in the MgH_2 matrix, thus creating a multielement, multiphase and multivalent environment, which not only largely favours the breaking and rebonding of H-H bonds and the transfer of electrons between H^- and Mg^{2+}, but also provide multiple hydrogen diffusion channels. These findings are of particularly scientific importance for the design and preparation of highly active catalysts for hydrogen storage in light-metal hydrides.

KEYWORDS: magnesium hydride; hydrogen storage; catalyst addition; ZrNi nanoparticles; disproportionation reaction

TOC Image

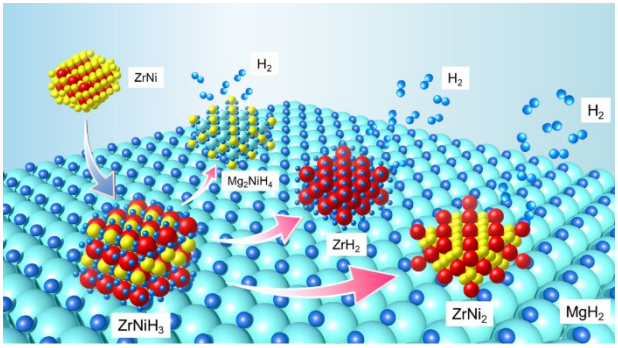

INTRODUCTION

Magnesium hydride (MgH_2), with high hydrogen capacity (7.6 wt.%), excellent reversibility, and natural abundance, has been attracting extensive research for advanced solid state hydrogen storage.[1-5] Nevertheless, the practical use of MgH_2 as a hydrogen reservoir is severely restricted by its stable thermodynamics and high kinetic barriers, which gives rise to the high operation temperatures for hydrogen storage. For example, a high temperature of 286 ºC is required to reach a desorption equilibrium pressure of 1 atm.[6-9] In the last several decades, great efforts have been made to improve the reaction thermodynamics and kinetics for storing hydrogen in Mg/MgH_2, including alloying, nanostructuring, catalyzing and compositing.[10-17]

In general, pure Mg at the micron sizes displays low reactivity toward H_2 molecules because it does not own *d*-band electrons that are particularly important to promote the dissociation of hydrogen molecules by interacting with the hydrogen antibonding orbital.[18,19] Furthermore, MgO or $Mg(OH)_2$ are readily generated on the surface of metallic Mg that hinder the dissociative adsorption of H_2 molecules or the transfer of H atoms from the surface to bulk.[6,20] An effective catalyst or catalytic additive has proved effective in improving hydrogen sorption kinetics of the Mg/MgH_2 system.[9,21,22] Typically, transition metals and their compounds including halides, oxides, carbides, nitrides and hydrides have been extensively studied for their capability to promote the breaking and rebonding of H-H and Mg-H bonds.[23,24] For example, Ti, Zr, Co, Fe, V, Nb and Ni are quite effective in expediting hydrogen storage process of Mg/MgH_2. It was demonstrated that 10 wt.% Ni nanoparticles modified MgH_2 started releasing hydrogen from 130 ºC.[25] Cui et al. revealed a strong dependence on the electronegativities of transition metals for the desorption performance of MgH_2, ranking from Ti, Nb, Ni, V, Co to Mo.[26] Edalati et al. observed rapid room-temperature hydrogenation of a Mg-Zr system prepared by a high pressure torsion process.[27] Liu

et al. demonstrated that 7.5 wt.% Nb- and 10.2 at% V-modified Mg rapidly absorbed 3.8-4.0 wt.% H_2 at 200 °C.[28,29] The addition of 5 wt.% 30-nm-thick Fe nanosheets decreased the desorption onset temperature of MgH_2 to ~182 °C and the absorption onset temperature to 75 °C.[30] When the absorption operated at 200 °C for 10 min, ~6 wt.% H_2 were recharged into the dehydrided sample.

Recently, alloys with multivalent elements have received intense attention for their synergistic effects, including $LaNi_5$, $ZrMn_2$, MoNi, FeCo, ZrNiPd, TiCrV, ZrFeCr, FeTiMn, etc. $ZrMn_2$ nanoparticles enabled the release of hydrogen from MgH_2 starting at ~182 °C and the total hydrogen release reached 6.7 wt.% when operating at 300 °C for 5 min.[31] It took 10 min and 60 s to desorb and absorb 6.7 wt.% H_2 by MoNi-modified MgH_2 sample at 300 °C, respectively.[32] Similarly, MgH_2 modified with nano-FeCo desorbed hydrogen starting from 200 °C and ending at 320 °C. When operating at 300 °C for 1 min, the dehydrided sample displayed a rapid hydrogen uptake because of the absorption of 6.7 wt.% H_2.[33] With 5 wt.% $Zr_{70}Ni_{20}Pd_{10}$, the full dehydrogenation and rehydrogenation of MgH_2 were achieved when operating at 200 °C/3.8 min and 100 °C/1.18 min, respectively. The measured H_2 capacity was 6 wt.%.[34] The hydride of nanocrystalline Mg with 20 wt.% $Ti_{0.16}Cr_{0.24}V_{0.6}$ liberated 5.67 wt.% H_2 under 0.1 bar H_2 when operating at 270 °C for 20 min .[35] By directly hydriding $Mg_{80}Ce_{18}Ni_2$, a $CeH_{2.73}$-MgH_2-Ni nanocomposite with remarkable hydrogen storage properties was fabricated *in situ*.[36] This nanocomposite featured numerous in-situ generated Ni nanoparticles, high density grain boundaries in nanocrystalline MgH_2, and interfaces between $CeH_{2.73}$ and MgH_2, functioned as nucleation sites of hydrides and H diffusion channels. Simultaneously, the *in situ* formed $CeH_{2.73}$/CeH_2 and metallic Ni phases are very fine and homogeneously dispersed in the MgH_2 matrix, which not only provide additional active sites but also favour the transfer of electrons between H^- and Mg^{2+}. A combined hydrogen spillover and hydrogen pump effect was attained

during dehydrogenation/rehydrogenation of Mg@Pt core–shell nanocomposites.[37] During hydrogenation process, the "spillover" effect contributed by Pt on Mg particles led to H-stabilized Mg_3Pt. In the follow-up dehydrogenation of MgH_2, the H-stabilized Mg_3Pt worked as a "hydrogen pump" and transformed back to Pt after desorption. As a result, we believe that the *in-situ* generation of nanosized multiphase and multivalent catalysts with excellent homogeneity is preferable for enhancing the hydrogen absorption/desorption reaction kinetics of Mg/MgH_2 system.

In this study, we synthesized nanoparticulate ZrNi (denoted as nano-ZrNi) with 10-60 nm in size by an improved co-precipitation and molten-salt reduction process. Hydrogen-driven disproportionation reaction of nano-ZrNi takes place upon hydriding, and uniformly dispersed ZrH_2, Mg_2NiH_4 and $ZrNi_2$ are formed *in situ* in the MgH_2 matrix, creating a multiphase, multivalent chemical environment and multi-channel H diffusion, consequently favouring the dissociation and recombination of H_2 molecules at the surface and the diffusion of H atoms inside the particles, respectively. This effectively decreases the activation energy barrier for hydrogen storage in Mg/MgH_2, and subsequently reduces the desorption/absorption temperatures and enhances the reaction kinetics. The presence of 7 wt.% nano-ZrNi enabled 6.1 wt.% of practical hydrogen capacity with ~178 °C of onset desorption temperature, reduced by 99 ºC relative to the pristine MgH_2. The dehydrided sample started absorbing H_2 at room temperature, and the total amount of H_2 uptake was measured to be 5.5 wt.% within 8 min at 150 ºC.

EXPERIMENTAL SECTIONS

Sample Preparation. All solvents and reagents used here were commercial. ZrNi nanoparticles were prepared by an improved co-precipitation and molten-salt reduction process. In a typical experiment, 0.233 g $ZrCl_4$ (1 mmol) and 0.1296 g (1 mmol) $NiCl_2$ were dissolved by using 10 mL deionized water, and then mixed with 10 mL NaOH (4 mol/L) under vigorous stirring (~600 rpm).

The hydroxide precipitate was collected after centrifuging and washing twice with deionized water and then freeze-drying at -40 ºC overnight (Fd-1B-80, BIOCOOL, China). Subsequently, the obtained hydroxide was grounded into powders and mixed with 2 g CaH_2 and 4 g KCl inside an high-purity argon-circulated glove box, which were then transferred into a custom-made Ni crucible, and put into a tube furnace for molten-salt reduction at 600 ºC for 3 h with the protection of high-purity Ar atmosphere. The resultant mixture was further washed under Ar protection to remove the residual KCl, CaH_2 and CaO with 0.1 mol/L acetic acid. ZrNi nanoparticles were collected after centrifugation, washing three times with deionized water and one more time with absolute ethanol and finally freeze-drying in vacuum. As a reference, bulk ZrNi alloy was prepared with 99.99% purity metals through induction-levitation melting under a continuous argon flow using a water-cooled copper crucible. To ensure a high homogeneity, the alloy ingot was turned over and re-melted three times. The obtained ingot was mechanically crushed and ground to powders of 200 mesh size (~75 μm) for use.

MgH_2 was synthesized by ball milling and heating 20-100 mesh Mg powders (Macklin, purity 98%) under 20 bar H_2 pressure at 340 °C for 12 h. The prepared ZrNi nanoparticles were ball milled with MgH_2 to obtain MgH_2 + *x* wt.% nano-ZrNi composites by using a QM-3SP4 planetary ball mill (Nanjing). Here, the x values were 1, 3, 5, 7 and 10. The milling operation was carried out under 50 bar H_2 at 500 rpm for 12 h. The weight ratio of 120:1 for ball-to-sample was adopted. The handling and transfer of samples were performed inside an Etelux glove box (Lab 2000, China), By circulating with the high-pure Ar, the H_2O and O_2 concentrations were maintained less than 0.1 ppm.

Structural and Morphological Characterization. The structure and morphology were characterized by XRD (X-ray diffraction) analysis, SEM (scanning electron microscope) and TEM

(transmission electron microscopy) observations, respectively. A Rigaku MiniFlex 600 (Japan) operated at 40 kV and 15 mA with Cu K_α (λ = 1.5418 Å) radiation was used to record XRD data. The 1 and 10° min^{-1} scanning rates were adopted for Rietveld refinement and qualitative analysis, respectively. SEM observation was performed using a Hitachi SU8010. TEM observation was implemented using a FEI Tecnai G2 F20 S-TWIN, which was also used to obtain the results of HRTEM (high-resolution TEM), HAADF-STEM (high-angle annular dark-field scanning TEM) and EDS (energy dispersive X-ray spectroscopy). The XPS (X-ray photoelectron spectroscopy) spectra were collected with a ESCALAB 250Xi facility (Thermo Scientific) under 3.7×10^{-10} Torr of base pressure. The X-ray source was the monochromatic Al K_α (*hv*: 1486.6 eV). The calibration of XPS data was performed by using the adventitious C peak at 284.8 eV as the reference. XAFS (X-ray absorption fine structure) experiments were performed on beamline BL11B at the SSRF (Shanghai Synchrotron Radiation Facility). XAFS data of Ni *K*-edge were analyzed by the Athena and Artemis programs. These programs are based on the IFEFFIT package from FEFF 6.[38] Normalized $\mu(E)$ data and Fourier transforms of k^3-weigted EXAFS spectra were acquired directly from the Athena program. Artemis module was used to obtain the quantitative structural parameters by least square curve fitting. A platform-free Fortran executable for wavelet analysis HAMA was applied for the calculation and graphical output of EXAFS spectra.[39]

Property Evaluation. A custom-designed TPD (Temperature-programmed desorption) system was employed to investigate hydrogen desorption behavior. The system was equipped with a Hiden QIC-20 gas analyzer (mass spectrometer, MS, England). The quantities of hydrogen desorption and absorption were measured through pressure-composition-temperature (PCT) as well as isothermal and non-isothermal methods on a homemade Sievert's type equipment. The experiments were conducted with approximately 50 mg of sample. For non-isothermal operations,

the stainless-steel reactor was gradually heated up by a resistance furnace under vacuum with a heating rate of 2 °C min^{-1} . For isothermal operations, the testing sample was rapidly heated at 10 °C min^{-1} to a preset temperature and kept at this temperature until the whole measurement was completed. Hydrogenation was performed under 50 bar H_2 pressure.

RESULTS AND DISCUSSION

Synthesis and characterization of ZrNi nanoparticles. The preparation of ZrNi nanoparticles is schematically illustrated in **Figure 1**a. The hydroxides of Zr and Ni are first precipitated by reacting $ZrCl_4$ and $NiCl_2$ with NaOH in water solution (**Equation 1**). After that, the hydroxide precipitates are mixed with KCl and CaH_2 and then heated to 600 ºC to realize a reduction reaction in molten salt (**Equation 2**). Here, the excessive KCl and CaH_2 form a KCl-$CaCl_2$ eutectic system, which not only accelerates the mass transport but also effectively prevents the aggregation and growth of the resultant ZrNi product, thus resulting in nanoparticles.[40]

$$ZrCl_4 + NiCl_2 + 6NaOH \rightarrow Zr(OH)_4 \downarrow + Ni(OH)_2 \downarrow + 6NaCl \quad (1)$$

$$Zr(OH)_4 + Ni(OH)_2 + 3CaH_2 \xrightarrow[600^o C]{KCl-CaCl_2} ZrNi + 3CaO + 6H_2O \quad (2)$$

The obtained ZrNi powders were first subjected to structure and morphology characterizations. The obtained experimental results are shown in **Figure 1**b-g. SEM observations clearly indicate nanoparticle morphology for the co-precipitation and molten-salt reduction products (**Figure 1**b), which were determined to be from 10 to 60 nm in size by TEM images (**Figure 1**c). Through statistical analysis with a Nano Measure software, the average particle size was calculated to be ~27.7 nm (the inset of **Figure 1**c). In stark contrast, the bulk sample prepared by induction-levitation melting and mechanical crushing displays typical microparticle morphology with 50-100 μm in size (**Figure 1**d). **Figure 1**e demonstrates very identical XRD patterns for both the

nanoparticle and the bulk samples, which agree well with the orthorhombic ZrNi (PDF 03-065-7465). HRTEM image (**Figure 1**f) confirms the orthorhombic ZrNi for the nanoparticle sample because fringes with interplanar spacings of 2.12, 2.33 and 2.48 Å can be identified (**Figure 1**g), which correspond to the (041), (-130) and (111) crystal planes, respectively. The corresponding FFT image of the highlighted area in **Figure 1**f is shown as the inset of **Figure 1**g. These results demonstrate that ZrNi nanoparticles can be synthesized by the combined co-precipitation and molten-salt reduction, which is denoted as nano-ZrNi hereinafter.

Catalytic activity of nano-ZrNi on MgH_2. The obtained nano-ZrNi was ball milled with MgH_2 at weight percentages of x =1, 3, 5, 7 and 10 wt.% to evaluate its catalytic activity. **Figure 2**a shows the TPD curves of MgH_2 + x wt.% ZrNi, which proves that nano-ZrNi induces a dramatic low-temperature shift in the dehydrogenation of MgH_2. The level of decrease in the desorption peak temperature strongly depends on the amount of nano-ZrNi, from 323 to 274 °C after adding 1 wt.% nano-ZrNi, and to 238 °C when 7 wt.% nano-ZrNi was added. This corresponds to a reduction of 85 °C. Remarkable reduction in the desorption temperatures was further confirmed by the volumetric release measurements. As shown in **Figure 2**b, pristine MgH_2 started releasing hydrogen at ~277 ºC and ~7.5 wt.% H_2 was desorbed at 360 ºC. In contrast, with the presence of 7 wt.% nano-ZrNi, the desorption onset temperature was significantly lowered to ~204 ºC and hydrogen release amounted to 6.5 wt.% at 275 ºC. Such dehydrogenation properties are also superior to the bulk-ZrNi-modified MgH_2 system (**Figure 2**c). More importantly, the onset desorption temperature was further reduced to 178 ºC in the second cycle (**Figure 2**d), which is decreased by 99 ºC relative to the pristine MgH_2. This further decrease is related to the change in the chemical states of catalytic species. It is noted that, however, the total dehydrogenation capacities of nano-ZrNi-containing samples are slightly lower than the theoretical values

calculated according to the addition amount of the catalyst. This is mainly ascribed to the oxygen contamination in the prepared nano-ZrNi, which give rise to the formation of MgO as discussed below.

Isothermal desorption results display a largely enhanced kinetics for the nano-ZrNi-catalyzed MgH_2. As observed in **Figure 2**e, MgH_2 with 7 wt.% nano-ZrNi rapidly liberated 6.1 wt.% H_2 when operating at 250 ºC for 10 min while nearly no hydrogen liberation was found for the pristine sample. More importantly, the 7 wt.% nano-ZrNi-containing MgH_2 desorbed 2.3 wt.% H_2 even operating at 200 °C for 30 min. The reaction kinetics of hydrogen desorption from MgH_2 + 7 wt.% nano-ZrNi is dramatically superior to Zr and Ni compounds-containing MgH_2 systems reported so far (**Figure 2**f).[41-48] However, the saturated hydrogen desorption amount at 200 ºC is much lower than that at 250 ºC, which is reasonably attributed to the limitation of the equilibrium pressure in the closed measurement system (**Figure S1**).[12]

Figure 3a compares the hydrogenation curves of dehydrogenated MgH_2 with different ZrNi alloys under an initial hydrogen pressure of 50 bar. Hydrogen uptake by the pristine sample started at approximately 100 °C. After adding 7 wt.% bulk-ZrNi, the hydrogenation onset temperature of was decreased to approximately 50 °C. With the presence of nano-ZrNi, hydrogen uptake was observed even at room temperature (25 ºC). Isothermal hydrogenation measurements indicate that at 150 °C, ~5.5 wt.% H_2 was charged rapidly into the dehydrided nano-ZrNi-modified sample within 8 min (**Figure 3**b). Under identical conditions, however, only ~0.7 wt.% H_2 was reabsorbed by the dehydrided pristine sample. When operation at 100 °C for 60 min, the nano-ZrNi-modified sample absorbed 4.8 wt.% H_2. It could also take up 3.9 wt.% H_2 when keeping for enough time (**Figure 3**c) even at 25 ºC. A much faster hydrogen uptake rate was also observed in the isothermal mode for the nano-ZrNi modified sample in comparison with those of bulk-ZrNi modified sample

and pristine MgH_2 (**Figure 3**d). All these indicate a remarkably improved hydrogenation capability at lowered temperatures, reasonably due to the high catalytic activity of ZrNi alloy as evidenced by the fact that that it readily absorbs nearly 2 wt.% H_2 at ambient temperature.[49] Moreover, nano-ZrNi particles are more homogeneously distributed in the composite sample as can be seen from the EDS mapping analyses (**Figure 4**), which are typically beneficial in catalyzing (de)hydrogenation.

Hydrogen Storage Thermodynamics and kinetics of nano-ZrNi-containing MgH_2. To understand the improved hydrogen storage properties of the nano-ZrNi modified MgH_2, the reaction thermodynamics and kinetics were further studied and compared. **Figure 5**a shows the measured PCI curves of the MgH_2 + 7 wt.% nano-ZrNi at 250-330 °C. The corresponding equilibrium pressures at 250, 275, 300 and 330 °C were determined to be 0.043, 0.093, 0.177 and 0.384 MPa, respectively. By applying van't Hoff equation, the calculated enthalpy change (ΔH) for the desorption reaction was 71.6 ± 1.0 kJ/mol-H_2 (**Figure 5**b), which is very closed to the theoretical value of pristine MgH_2 (~76 kJ/mol-H_2).[50] This result indicates that the reaction thermodynamics of hydrogen desorption from MgH_2 has not been appreciably changed through the addition of nano-ZrNi. As a result, it is believed that the reduced temperatures for hydrogen storage in the nano-ZrNi modified MgH_2 is mainly attributed to the decreased activation energy barriers. By fitting the Kissinger's plots derived from the correlation between the peak temperature and heating rate (**Figure 5**c), the activation energy values can be calculated and compared, which are 88.6 ± 4.3 kJ mol^{-1} for the nano-ZrNi modified MgH_2 samples and 151.3 ± 14.1 kJ mol^{-1} for the pristine MgH_2 (**Figure 5**d), indicating a ~40% reduction in the kinetic barrier of dehydrogenation by nano-ZrNi.

Chemical states of catalytic active species. Through XRD and XPS analyses, the chemical compositions and states of the catalytic species during ball milling and hydrogen storage processes were studied. **Figure 6** shows XRD profiles of the nano-ZrNi modified MgH_2 at different stages. After ball milling under 50 bar H_2, the characteristic reflections of orthorhombic $ZrNiH_3$ phase (PDF 01-089-2626) were identified (**Figure 6**a), which agrees well with the previous report,[51] in addition to α-MgH_2 (PDF 01-075-7944). After dehydrogenation, MgH_2 was converted to metallic Mg as expected and the diffraction peaks of cubic $ZrNi_2$ phase (PDF 01-072-2676) were detected (**Figure 6**b). Subsequent hydrogenation induced the formation of α-MgH_2, γ-MgH_2, Mg_2NiH_4, ZrH_2 and $ZrNi_2$, as indicated by XRD profile and Rietveld refinement in **Figure 6**c. In addition, MgO was identified as an impurity in the dehydrogenated and rehydrogenated samples, which is responsible for the slightly lower practical hydrogen capacity related to the theoretical values as mentioned above. High resolution XPS spectra provided evidence on the change of chemical states of Zr. As shown in **Figure 7**a, Zr 3d XPS peaks in the prepared catalyst can be assigned to ZrNi (179.2/181.6 eV) and ZrO_2 (183.6/186.0 eV).[52] Here, the presence of ZrO_2 explains the formation of MgO upon hydrogen cycling as observed in XRD patterns (**Figure 6**). After ball milling with MgH_2 under 50 bar H_2, the Zr 3d XPS peaks display a slight high-energy shift from 179.2 and 181.6 eV to 179.5 and 181.9 eV, due to the formation of $ZrNiH_3$ as observed by XRD. Six peaks were resolved from the Zr 3d XPS spectrum of the post-dehydrided sample in the first cycle. In addition to ZrO_2 peaks,[53] the doublets at 179.3/181.7 and 180.1/182.4 eV can be ascribed to $ZrNi_2$ and ZrH_2,[54,55] respectively, which are still visible after subsequent hydrogenation. These results indicate the disproportionation reaction of ZrNi during the 1st dehydrogenation and hydrogenation.

Furthermore, XAFS examinations were carried out to reveal the evolution tendency of Ni-based species. **Figure 7**b presents the XANES (X-ray absorption near-edge structure) spectra. With

respect to the dehydrogenated sample, the XANES spectrum of Ni moved to the higher energy despite a very similar shape, indicating a much stronger bonding energy of Ni with the most neighbor atoms caused by the presence of H after hydrogenation. Interestingly, the extended X-ray absorption fine structure (EXAFS) displays only one strong peak at the first coordination shell of Ni (**Figure 7**c), possibly due to the nearly identical contacting radius of Mg (0.160 nm) and Zr (0.158 nm) atoms.[56] More importantly, the overlapping peaks of the first coordination shell of Ni atoms for the dehydrogenated and rehydrogenated samples confirm their nearly identical bond length with the neighbor atoms. This is well agreed by the wavelet transform (WT) analysis of the k^3-weighted EXAFS signals (**Figure 7**d). All these agree well with the XRD and XPS results. As a result, we believe that the hydrogenation induces a slight change in the local electronic structure of Ni atoms but does not affect the surrounding atomic arrangement.

According to the abovementioned discussion, the following chemical events can be deduced upon ball milling and de-/hydrogenation.

Ball milling:

$$MgH_2 + ZrNi \xrightarrow[BM]{50\ bar\ H_2} MgH_2 + ZrNiH_3 \qquad (3)$$

1st dehydrogenation:

$$MgH_2 + ZrNiH_3 \xrightarrow[de]{275^oC} \frac{1}{3}Mg + \frac{1}{3}ZrNi_2 + \frac{2}{3}ZrH_2 + \frac{1}{3}Mg_2Ni + \frac{11}{6}H_2 \qquad (4)$$

1st rehydrogenation:

$$Mg + ZrNi_2 + ZrH_2 + Mg_2Ni + 3H_2 \xrightarrow[hy]{250^oC} MgH_2 + ZrH_2 + Mg_2NiH_4 + ZrNi_2 \qquad (5)$$

After ball milling and first desorption/absorption cycle, a multiphase and multivalent chemical environment was created successfully. This was further confirmed by HAADF-STEM observation and EDS mapping analyses because ZrH_2, Mg_2NiH_4, $ZrNi_2$ were also speculated through analyzing

the EDS mapping of Zr and Ni shown in **Figure 8**, together with XRD results, which were uniformly dispersed in the MgH_2 matrix. Such chemical environment not only favours the breaking and rebonding of H-H bonds and the transfer of electrons between H^- and Mg^{2+},[57-59] but also provide multiple hydrogen diffusion channels,[60-62] which are schematically illustrated in **Figure 9**. All these works together leading to remarkably reduced operation temperatures and enhanced kinetics for storing hydrogen in nano-ZrNi-modified MgH_2.

Volumetric hydrogen storage density and cycling stability. To obtain a practically high volumetric hydrogen density, a pellet with 12.791 mm in diameter was made by cold pressing 203 mg of sample powders (**Figure 10**a). Attractively, the pellet fabricated under 800 MPa has isothermal dehydrogenation behavior similar to that of powder sample (**Figure 10**b). The calculated volumetric hydrogen storage density was ~75.5 g H_2 L^{-1} as it released ~6.14 wt.% H_2 while heated to 250 ºC. This volumetric hydrogen density value is remarkably higher than the ultimate goal (50 g H_2 L^{-1}) set by US Department of Energy for on-board applications.[63]

Moreover, the cyclability of the MgH_2 + 7 wt.% nano ZrNi sample was also evaluated in the powder and pellet forms. The hydrogen desorption/absorption were measured isothermally at 250 ºC. The results are demonstrated in **Figure 10**c,d and **Figure S2**. It is discovered that after activation, no appreciable degradation in the hydrogen capacity and the reaction kinetics was observed. After 10 desorption/absorption cycles, the hydrogen capacity still stayed at 6.1 wt.% with nearly unchanged de-/hydriding rate (**Figure S3** and **S4**), indicating a good cycling durability. The stable cyclability is particularly favorable for the practical hydrogen storage applications, and it can be attributed to the uniform distribution of active catalytic species without segregation even after 10 desorption/absorption cycles (**Figure S5**).

CONCLUSION

In this paper, 10-60 nm-sized nanoparticulate ZrNi was successfully synthesized by means of co-precipitation followed by molten-salt reduction. As a precursor, the resultant nano-ZrNi leads to species with superior catalytic activity toward hydrogen storage by Mg/MgH_2. When ball milled with MgH_2, ZrNi was first converted to $ZrNiH_3$. After 1st de-/hydriding cycle, ZrH_2, Mg_2NiH_4 and $ZrNi_2$ are *in situ* produced due to the disproportionation reaction of ZrNi. Such multielement, multiphase and multivalent environment not only favours the breaking and rebonding of H-H bonds and the transfer of electrons between H^- and Mg^{2+}, but also provides multiple hydrogen diffusion channels. All these result in ~ 40% reduction in the dehydrogenation apparent activation energy barrier, effectively lowering the operation temperatures and increasing the reaction kinetics for storing hydrogen in Mg/MgH_2. The 7 wt.% nano-ZrNi modified MgH_2 started desorbing hydrogen at ~178 °C. When operating at 250 °C for 10 min, approximately 6.1 wt.% of H_2 was detached. At room temperature (25 ºC) under 50 bar H_2, the dehydrogenated sample started absorbing hydrogen and the total amount of H_2 uptake increased to 5.5 wt.% when operating at 150 °C for 8 min. After 10 desorption/absorption cycles, the practical hydrogen capacity still stayed at 6.1 wt.%, which can be attributed to the uniform distribution of catalytic active species and their stable chemical states.

ASSOCIATED CONTENT

Supporting Information

Isothermal dehydrogenation at 200 ºC; Cycling behaviors of pellet sample; Isothermal desorption and absorption curves of powder and pellet samples upon cycling; SEM images and EDS mappings of Mg, Zr and Ni for the powder and pellet samples before and after 10 cycles. (PDF)

AUTHOR INFORMATION

Corresponding Author

Yongfeng Liu − State Key Laboratory of Silicon and Advanced Semiconductor Materials, Key Laboratory of Advanced Materials and Applications for Batteries of Zhejiang Province and School of Materials Science and Engineering, Zhejiang University, Hangzhou 310058, China; Taizhou Institute of Zhejiang University, Taizhou 318000, China; Institute of Science and Technology for New Energy, Xi'an Technological University, Xi'an, 710021, China; Email: mselyf@zju.edu.cn

Fang Fang − Department of Materials Science, Fudan University, Shanghai, 200433 China; Email: f_fang@fudan.edu.cn

Hongge Pan − State Key Laboratory of Silicon and Advanced Semiconductor Materials, Key Laboratory of Advanced Materials and Applications for Batteries of Zhejiang Province and School of Materials Science and Engineering, Zhejiang University, Hangzhou 310058, China; Institute of Science and Technology for New Energy, Xi'an Technological University, Xi'an, 710021, China; Email: hgpan@zju.edu.cn

Authors

Lingchao Zhang – State Key Laboratory of Silicon and Advanced Semiconductor Materials, Key Laboratory of Advanced Materials and Applications for Batteries of Zhejiang Province and School of Materials Science and Engineering, Zhejiang University, Hangzhou 310058, China

Xin Zhang – State Key Laboratory of Silicon and Advanced Semiconductor Materials, Key Laboratory of Advanced Materials and Applications for Batteries of Zhejiang Province and School

of Materials Science and Engineering, Zhejiang University, Hangzhou 310058, China; Taizhou Institute of Zhejiang University, Taizhou 318000, China

Wenxuan Zhang – State Key Laboratory of Silicon and Advanced Semiconductor Materials, Key Laboratory of Advanced Materials and Applications for Batteries of Zhejiang Province and School of Materials Science and Engineering, Zhejiang University, Hangzhou 310058, China

Zhenguo Huang – School of Civil & Environmental Engineering, University of Technology Sydney, 81 Broadway, Ultimo, NSW, 2007, Australia

Fang Fang – Department of Materials Science, Fudan University, Shanghai, 200433 China

Juan Li – College of Materials Science and Engineering, Zhejiang University of Technology, Hangzhou, 310014, China

Limei Yang – School of Civil & Environmental Engineering, University of Technology Sydney, 81 Broadway, Ultimo, NSW, 2007, Australia

Changdong Gu – State Key Laboratory of Silicon and Advanced Semiconductor Materials, Key Laboratory of Advanced Materials and Applications for Batteries of Zhejiang Province and School of Materials Science and Engineering, Zhejiang University, Hangzhou 310058, China.

Wenping Sun – State Key Laboratory of Silicon and Advanced Semiconductor Materials, Key Laboratory of Advanced Materials and Applications for Batteries of Zhejiang Province and School of Materials Science and Engineering, Zhejiang University, Hangzhou 310058, China.

Mingxia Gao – State Key Laboratory of Silicon and Advanced Semiconductor Materials, Key Laboratory of Advanced Materials and Applications for Batteries of Zhejiang Province and School of Materials Science and Engineering, Zhejiang University, Hangzhou 310058, China.

Author Contributions

L.Z. conceived of and conducted experiments and wrote the draft manuscript; X.Z. provided suggestions on the experiments and gave help in writing original draft; W.Z. gave helpful discussions for formal analysis and participated in the experiment; Z.H. gave valuable comments for formal analysis and contributed to writing, reviewing and editing the draft manuscript; F.F. carried out theoretical research and contributed to writing, reviewing and editing the draft manuscript; J.L., L.Y. and C.G. gave helpful discussions for formal analysis; W.S. gave helpful comments for formal analysis and provided guidance of XAFS measurements; M.G. provided guidance of analytical methods, experimental design and academic approaches; H.P. provided guidance of analytical methods and academic resources; Y.L. provided guidance of analytical methods, experimental design and academic resources, carried out theoretical research, writing, reviewing and editing the draft manuscript.

NOTES

The authors declare no competing financial interest.

ACKNOWLEDGMENTS

We gratefully acknowledge the financial support received from the National Key R&D Program of China (2022YFB3803700), the National Outstanding Youth Foundation of China (52125104), the Natural Science Foundation of Zhejiang Province (LD21E010002), the National Natural Science Foundation of China (52001277, U22A20120), the Fundamental Research Funds for the Central Universities (2021FZZX001-09, 226-2022-00246), and the National Youth Top-Notch Talent Support Program. The authors thank the staff of beamline BL11B at the Shanghai Synchrotron Radiation Facility (SSRF) for their support in XAFS measurements. The authors

thank Dr. Yangfan Lu (School of Materials Science and Engineering at Zhejiang University) for her help on XPS measurement and analysis.

REFERENCES

(1) Schlapbach, L.; Züttel, A. Hydrogen-storage materials for mobile applications. *Nature* **2001**, *414*, 353-358.

(2) Allendorf, M. D.; Stavila, V.; Snider, J. L.; Witman, M.; Bowden, M. E.; Brooks, K.; Tran, B. L.; Autrey, T. Challenges to developing materials for the transport and storage of hydrogen. *Nat. Chem.* **2022**, *14*, 1214-1223.

(3) Yartys, V. A.; Lototskyy, M. V.; Akiba, E.; Albert, R.; Antonov, V. E.; Ares, J. R.; Baricco, M.; Bourgeois, N.; Buckley, C. E.; Bellosta von Colbe, J. M.; Crivello, J. C.; Cuevas, F.; Denys, R. V.; Dornheim, M.; Felderhoff, M.; Grant, D. M.; Hauback, B. C.; Humphries, T. D.; Jacob, I.; Jensen, T. R.; de Jongh, P. E.; Joubert, J. M.; Kuzovnikov, M. A.; Latroche, M.; Paskevicius, M.; Pasquini, L.; Popilevsky, L.; Skripnyuk, V. M.; Rabkin, E.; Sofianos, M. V.; Stuart, A.; Walker, G.; Wang, H.; Webb, C. J.; Zhu, M. Magnesium based materials for hydrogen based energy storage: Past, present and future. *Int. J. Hydrogen Energy* **2019**, *44*, 7809-7859.

(4) Ouyang, L. Z.; Liu, F.; Wang, H.; Liu, J. W.; Yang, X. S.; Sun L. X.; Zhu, M. Magnesium-based hydrogen storage compounds: A review. *J. Alloys Compd.* **2020**, *832*, 154865.

(5) Lu, J.; Choi, Y. J.; Fang, Z. Z.; Sohn, H. Y.; Ronnebro, E. Hydrogenation of Nanocrystalline Mg at Room Temperature in the Presence of TiH_2. *J. Am. Chem. Soc.* **2010**, *132*, 6616-6617.

(6) Selvam, P.; Viswanathan, B.; Swamy, C. S.; Srinivasan, V. Magnesium and magnesium alloy hydrides. *Int. J. Hydrogen Energy* **1986**, *11*, 169-192.

(7) Sun, Y. H.; Shen, C. Q.; Lai, Q. W.; Liu, W.; Wang, D. W.; Aguey-Zinsou, K. F. Tailoring magnesium based materials for hydrogen storage through synthesis: Current state of the art. *Energy Storage Mater*. **2018**, *10*, 168-198.

(8) Mandal, T. K.; Gregory, D. H. Hydrogen: A future energy vector for sustainable development. *Proc. Inst. Mech. Eng., Part C*. **2010**, *224*, 539-558.

(9) Aguey-Zinsou, K. F.; Ares-Fernandez, J. R. Hydrogen in magnesium: new perspectives toward functional stores. *Energy Environ. Sci.* **2010**, *3*, 526-543.

(10) Singh, A. K.; Singh, A. K.; Srivastava, O. N. On the synthesis of the Mg_2Ni alloy by mechanical alloying. *J. Alloys Compd.* **1995**, *227*, 63-68.

(11) Abe, J. O.; Popoola, A. P. I.; Ajenifuja, E.; Popoola, O. M. Hydrogen energy, economy and storage: Review and recommendation. *Int. J. Hydrogen Energy* **2019**, *44*, 15072-15086.

(12) Zhang, X.; Liu, Y. F.; Ren, Z. H.; Zhang, X. L.; Hu, J. J.; Huang, Z. G.; Lu, Y. H.; Gao, M. X.; Pan, H. G. Realizing 6.7 wt% reversible storage of hydrogen at ambient temperature with non-confined ultrafine magnesium hydrides. *Energy Environ. Sci.* **2021**, *14*, 2302-2313.

(13) Barkhordarian, G.; Klassen, T.; Bormann, R. Fast hydrogen sorption kinetics of nanocrystalline Mg using Nb_2O_5 as catalyst. *Scripta Mater.* **2003**, *49*, 213-217.

(14) Zhang, J. F.; Li, Z. N.; Wu, Y. F.; Guo, X. M.; Ye, J. H.; Yuan, B. L.; Wang, S. M.; Jiang, L. J. Recent advances on the thermal destabilization of Mg-based hydrogen storage materials. *Rsc Advances* **2019**, *9*, 408-428.

(15) Xie, X. B.; Chen, M.; Hu, M. M.; Wang, B. L.; Yu, R. H.; Liu, T. Recent advances in magnesium-based hydrogen storage materials with multiple catalysts. *Int. J. Hydrogen Energy* **2019**, *44*, 10694-10712.

(16) Zhang, J.; Yan, S.; Qu, H. Recent progress in magnesium hydride modified through catalysis and nanoconfinement. *Int. J. Hydrogen Energy* **2018**, *43*, 1545-1565.

(17) Crivello, J. C.; Dam, B.; Denys, R. V.; Dornheim, M.; Grant, D. M.; Huot, J.; Jensen, T. R.; de Jongh, P. E.; Latroche, M.; Milanese, C.; Milčius, D.; Walker, G. S.; Webb, C. J.; Zlotea, C.; Yartys, V. A. Review of magnesium hydride-based materials: development and optimisation. *Appl. Phys. A: Mater. Sci. Process.* **2016**, *122*, 1-20.

(18) Uchida, H.; Ohtani, Y.; Ozawa, M.; Kawahata, T.; Suzuki, T. Surface processes of H_2 in the initial activation of $LaNi_5$. *J. Less Common Met.* **1991**, *172*, 983-996.

(19) Christmann, K. Some General Aspects of Hydrogen Chemisorption on Metal Surfaces. *Prog. Surf. Sci.* **1995**, *48*, 15-26.

(20) Jain, I.; Lal, C.; Jain, A. Hydrogen storage in Mg: A most promising material. *Int. J. Hydrogen Energy* **2010**, *35*, 5133-5144.

(21) Sakintuna, B.; Lamari-Darkrim, F.; Hirscher, M. Metal hydride materials for solid hydrogen storage: A review. *Int. J. Hydrogen Energy* **2007**, *32*, 1121-1140.

(22) van den Berg, A. W. C.; Areán, C. O. Materials for hydrogen storage: current research trends and perspectives. *Chem. Commun.* **2008**, *6*, 668-681.

(23) Salman, M. S.; Pratthana, C.; Lai, Q. W.; Wang, T.; Rambhujun, N.; Srivastava, K.; Aguey-Zinsou, K. F. Catalysis in Solid Hydrogen Storage: Recent Advances, Challenges, and Perspectives. *Energy Technol*. **2022**, *10*, 2200433.

(24) Zhang, X. L.; Liu, Y. F.; Zhang, X.; Hu, J. J.; Gao, M. X.; Pan, H. G. Empowering hydrogen storage performance of MgH_2 by nanoengineering and nanocatalysis. *Mater. Today Nano* **2020**, *9*, 100064.

(25) Yu, H.; Bennici, S.; Auroux, A. Hydrogen storage and release: Kinetic and thermodynamic studies of MgH_2 activated by transition metal nanoparticles. *Int. J. Hydrogen Energy*. **2014**, *39*, 11633-11641.

(26) Cui, J.; Liu, J. W.; Wang, H.; Ouyang, L. Z.; Sun, D. L.; Zhu, M.; Yao, X. D. Mg–TM (TM: Ti, Nb, V, Co, Mo or Ni) core–shell like nanostructures: synthesis, hydrogen storage performance and catalytic mechanism. *J. Mater. Chem. A* **2014**, *2*, 9645-9655.

(27) Edalati, K.; Emami, H.; Ikeda, Y.; Iwaoka, H.; Tanaka, I.; Akiba, E.; Horita, Z. New nanostructured phases with reversible hydrogen storage capability in immiscible magnesium-zirconium system produced by high-pressure torsion. *Acta Mater.* **2016**, *108*, 293-303.

(28) Liu, T.; Ma, X. J.; Chen, C. G.; Xu, L.; Li, X. G. Catalytic Effect of Nb Nanoparticles for Improving the Hydrogen Storage Properties of Mg-Based Nanocomposite. *J. Phys. Chem. C*. **2015**, *119*, 14029-14037.

(29) Liu, T.; Zhang, T. W.; Qin, C. G.; Zhu, M.; Li, X. G. Improved hydrogen storage properties of Mg–V nanoparticles prepared by hydrogen plasma–metal reaction. *J. Power Sources* **2011**, *196*, 9599-9604.

(30) Zhang, L. T.; Ji, L.; Yao, Z. D.; Yan, N. H.; Sun, Z.; Yang, X. L.; Zhu, X. Q.; Hu, S. L.; Chen, L. X. Facile synthesized Fe nanosheets as superior active catalyst for hydrogen storage in MgH_2. *Int. J. Hydrogen Energy* **2019**, *44*, 21955-21964.

(31) Zhang, L. T.; Cai, Z. L.; Yao, Z. D.; Ji, L.; Sun, Z.; Yan, N. H.; Zhang, B. Y.; Xiao, B. B.; Du, J.; Zhu, X. Q.; Chen, L. X. A striking catalytic effect of facile synthesized $ZrMn_2$ nanoparticles on the de/rehydrogenation properties of MgH_2. *J. Mater. Chem. A* **2019**, *7*, 5626-5634.

(32) Chen, M.; Pu, Y. H.; Li, Z. Y.; Huang, G.; Liu, X. F.; Lu, Y.; Tang, W. K.; Xu, L.; Liu, S. Y.; Yu, R. H.; Shui, J. L. Synergy between metallic components of MoNi alloy for catalyzing highly efficient hydrogen storage of MgH_2. *Nano Res*. **2020**, *13*, 2063-2071.

(33) Yang, X. L.; Ji, L.; Yan, N. H.; Sun, Z.; Lu, X.; Zhang, L. T.; Zhu, X. Q.; Chen, L. X. Superior catalytic effects of FeCo nanosheets on MgH_2 for hydrogen storage. *Dalton Trans.* **2019**, *48*, 12699-12706.

(34) El-Eskandarany, M. S. Metallic glassy $Zr_{70}Ni_{20}Pd_{10}$ powders for improving the hydrogenation/dehydrogenation behavior of MgH_2. *Sci. Rep.* **2016**, *6*, 1-13.

(35) Zhang, J. F.; Li, Z. N.; Wu, Y. F.; Guo, X. M.; Ye, J. H.; Yuan, B. L.; Yuan, H. P. Wang, S. M.; Jiang, L. J. Significant Thermodynamic Destabilization and Superior Hydrogen Storage Properties of Nanocrystalline Mg-20 wt % Ti−Cr−V_x (x = 0.4, 0.6, 0.8; Ti/Cr = 2:3) Composites Synthesized by Reactive Ball Milling. *J. Phys. Chem. C* **2019**, *123*, 15963-15976.

(36) Ouyang, L. Z.; Yang, X. S.; Zhu, M.; Liu, J. W.; Dong, H. W.; Sun, D. L.; Zou, J.; Yao, X. D. Enhanced Hydrogen Storage Kinetics and Stability by Synergistic Effects of in Situ Formed $CeH_{2.73}$ and Ni in $CeH_{2.73}$-MgH_2-Ni Nanocomposites. *J. Phys. Chem. C* **2014**, *118*, 7808-7820.

(37) Lu, C.; Ma, Y. L.; Li, F.; Zhu, H.; Zeng, X. Q.; Ding, W. J.; Deng, T.; Wu, J. B.; Zou, J. X. Visualization of fast "hydrogen pump" in core–shell nanostructured Mg@Pt through hydrogen-stabilized Mg_3Pt. *J. Mater. Chem. A* **2019**, *7*, 14629-14637.

(38) Ravel, B.; Newville, M. ATHENA, ARTEMIS, HEPHAESTUS: data analysis for X-ray absorption spectroscopy using IFEFFIT. *J. Synchrotron Radiat*. **2005**, *12*, 537-541.

(39) Funke, H.; Scheinost, A. C.; Chukalina, M. Wavelet analysis of extended x-ray absorption fine structure data. *Phys. Rev. B* **2005**, *71*, 094110.

(40) Yu, H. E.; Yang, X.; Jiang, X. J.; Wu, Y. M.; Chen, S. P.; Lin, W.; Wu, Y.; Xie, L.; Li, X. G.; Zheng, J. $LaNi_{5.5}$ particles for reversible hydrogen storage in N-ethylcarbazole. *Nano Energy* **2021**, *80*, 105476.

(41) Pighin, S. A.; Capurso, G.; Lo Russo, S.; Peretti, H. A. Hydrogen sorption kinetics of magnesium hydride enhanced by the addition of Zr_8Ni_{21} alloy. *J. Alloys Compd.* **2012**, *530*, 111-115.

(42) Yang, X. L.; Hou, Q. H.; Yu, L. B.; Zhang, J. Q. Improvement of the hydrogen storage characteristics of MgH_2 with a flake Ni nano-catalyst composite. *Dalton Trans*. **2021**, *50*, 1797-1807.

(43) Chen, M.; Wang, Y. Q.; Xiao, X. Z.; Lu, Y. H.; Zhang, M.; Zheng, J. G.; Chen, L. X. Highly efficient ZrH_2 nanocatalyst for the superior hydrogenation kinetics of magnesium hydride

under moderate conditions: Investigation and mechanistic insights. *Appl. Surf. Sci.* **2021**, *541*, 148375.

(44) Fu, Y. K.; Ding, Z. M.; Ren, S. Q.; Li, X. J.; Zhou, S. H.; Zhang, L.; Wang, W. F.; Wu, L. L.; Li, Y.; Han, S. M. Effect of in-situ formed Mg_2Ni/Mg_2NiH_4 compounds on hydrogen storage performance of MgH_2. *Int. J. Hydrogen Energy* **2020**, *45*, 28154-28162.

(45) El-Eskandarany, M. S.; Al-Matrouk, H.; Shaban, E.; Al-Duweesh, A. Superior catalytic effect of nanocrystalline big-cube Zr_2Ni metastable phase for improving the hydrogen sorption/desorption kinetics and cyclability of MgH_2 powders. *Energy* **2015**, *91*, 274-282.

(46) Dehouche, Z.; Peretti, H. A.; Hamoudi, S.; Yoo, Y.; Belkacemi, K. Effect of activated alloys on hydrogen discharge kinetics of MgH_2 nanocrystals. *J. Alloys Compd.* **2008**, *455*, 432-439.

(47) El-Eskandarany, M. S.; Shaban, E.; Al-Matrouk, H.; Behbehani, M.; Alkandary, A.; Aldakheel, F.; Ali, N.; Ahmed, S. A. Structure, morphology and hydrogen storage kinetics of nanocomposite MgH_2/10 wt% $ZrNi_5$ powders. *Mater. Today Energy* **2017**, *3*, 60-71.

(48) Dong, J. J.; Panda, S.; Zhu, W.; Zou, J. X.; Ding, W. J. Enhanced hydrogen sorption properties of MgH_2 when doped with mechanically alloyed amorphous $Zr_{0.67}Ni_{0.33}$ particles. *Int. J. Hydrogen Energy* **2020**, *45*, 28144-28153.

(49) Nei, J.; Young, K.; Regmi, R.; Lawes, G.; Salley, S. O.; Ng, K. Y. S. Gaseous phase hydrogen storage and electrochemical properties of Zr_8Ni_{21}, Zr_7Ni_{10}, Zr_9Ni_{11}, and ZrNi metal hydride alloys. *Int. J. Hydrogen Energy* **2012**, *37*, 16042-16055.

(50) Bogdanovic, B.; Bohmhammel, K.; Christ, B.; Reiser, A.; Schlichte, K.; Vehlen, R.; Wolf, U. Thermodynamic investigation of the magnesium–hydrogen system. *J. Alloys Compd.* **1999**, *282*, 84-92.

(51) Peterson, S. W.; Sadana, V. N.; Korst, W. L. Neutron diffraction study of nickel zirconium hydride. *J. Phys.* **1964**, *25*, 451-453.

(52) Kumar, L.; Sarma, D. D.; Krummacher, S. XPS study of the room temperature surface oxidation of zirconium and its binary alloys with tin, chromium and iron. *Appl. Surf. Sci.* **1988**, *32*, 309-319.

(53) Roustila, A.; Chene, J.; Severac, C. XPS study of hydrogen and oxygen interactions on the surface of the NiZr intermetallic compound. *Int. J. Hydrogen Energy* **2007**, *32*, 5026-5032.

(54) Walz, B.; Oelhafen, P.; Guntherodt, H.-J.; Baiker, A. Surface oxidation of amorphous Ni□Zr alloys. *Appl. Surf. Sci*. **1989**, *37*, 337-352.

(55) Riesterer, T. Electronic Structure and Bonding in Metal Hydrides, Studied with Photoelectron Spectroscopy. *Z. Phys. B: Condens. Matter*. **1987**, *66*, 441-458.

(56) Miracley, D. B.; Sanders, W. S. The influence of efficient atomic packing on the constitution of metallic glasses. *Philos. Mag.* **2003**, *83*, 2409-2428.

(57) Cui, J.; Wang, H.; Liu, J. W.; Ouyang, L. Z.; Zhang, Q. A.; Sun, D. L.; Yao, X. D.; Zhu, M. Remarkable enhancement in dehydrogenation of MgH_2 by a nano-coating of multi-valence Ti-based catalysts. *J. Mater. Chem. A* **2013**, *1*, 5603-5611.

(58) Zhang, L. T.; Xiao, X. Z.; Xu, C. C.; Zheng, J. G.; Fan, X. L.; Shao, J.; Li, S. Q.; Ge, H. W.; Wang, Q. D.; Chen, L. X. Remarkably Improved Hydrogen Storage Performance of MgH_2 Catalyzed by Multivalence NbH_x Nanoparticles. *J. Phys. Chem. C* **2015**, *119*, 8554-8562.

(59) El Khatabi, M.; Bhihi, M.; Naji, S.; Labrim, H.; Benyoussef, A.; El Kenz, A.; Loulidi, M. Study of doping effects with 3d and 4d-transition metals on the hydrogen storage properties of MgH_2. *Int. J. Hydrogen Energy* **2016**, *41*, 4712-4718.

(60) El-Eskandarany, M. S.; Shaban, E.; Ali, N.; Aldakheel, F.; Alkandary, A. In-situ catalyzation approach for enhancing the hydrogenation/ dehydrogenation kinetics of MgH_2 powders with Ni particles. *Sci. Rep.* **2016**, *6*, 37335.

(61) Chen, J.; Xia, G. L.; Guo, Z. P.; Huang, Z. G.; Liu, H. K.; Yu, X. B. Porous Ni nanofibers with enhanced catalytic effect on the hydrogen storage performance of MgH_2. *J. Mater. Chem. A* **2015**, *3*, 15843.

(62) Zou, J. X.; Long, S.; Chen, X.; Zeng, X. Q.; Ding, W. J. Preparation and hydrogen sorption properties of a Ni decorated Mg based Mg@Ni nano-composite. *Int. J. Hydrogen Energy* **2015**, *40*, 1820-1828.

(63) US Department of Energy, DOE Technical Targets for Onboard Hydrogen Storage for Light-Duty Vehicles. https://www.energy.gov/eere/fuelcells/doe-technical-targets-onboard-hydrogen-storage-light-duty-vehicles, US Washington DC, 2016.

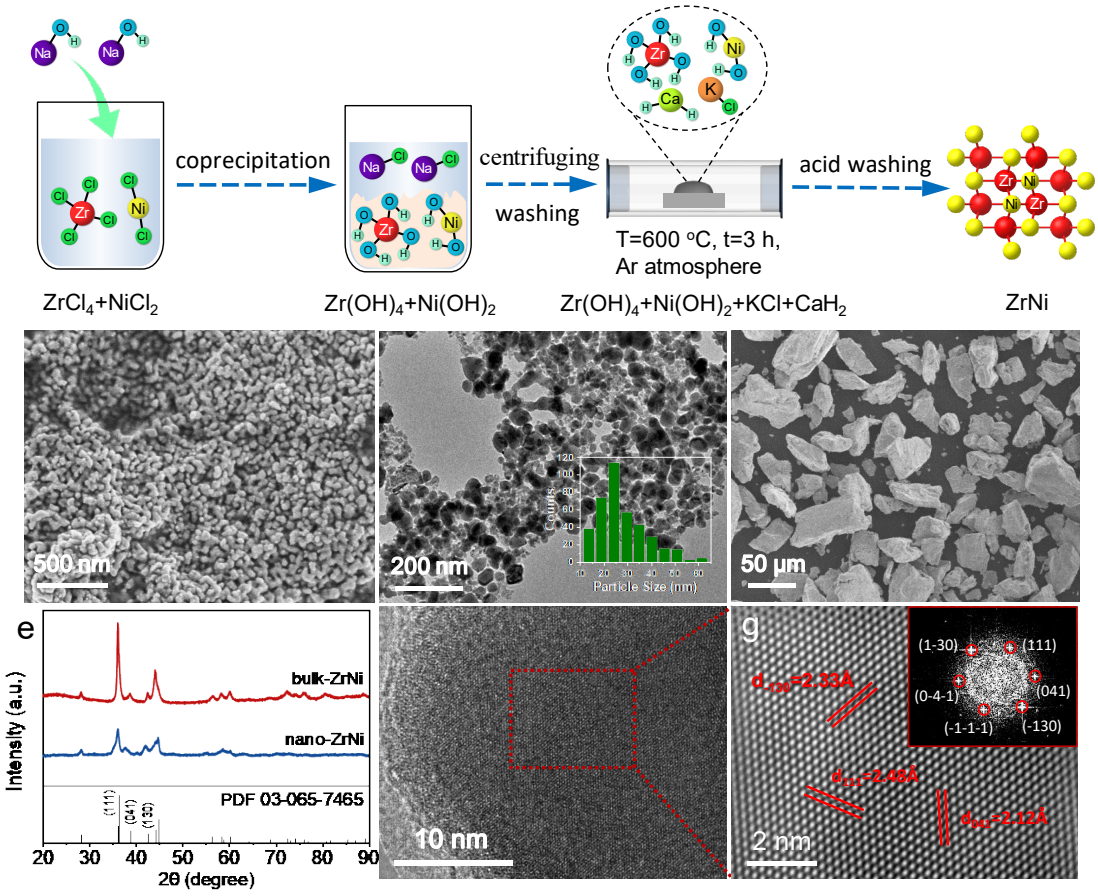

Figure 1. Schematic preparation of nano-ZrNi (a). SEM (b), TEM (c) images and particle size distribution (the inset of c) of nano-ZrNi. SEM (d) image of bulk ZrNi. XRD patterns (e) of ZrNi synthesized with different methods. HRTEM images (f), selected-area FFT pattern (inset of g) and inverse FFT pattern (g) of prepared nano-ZrNi.

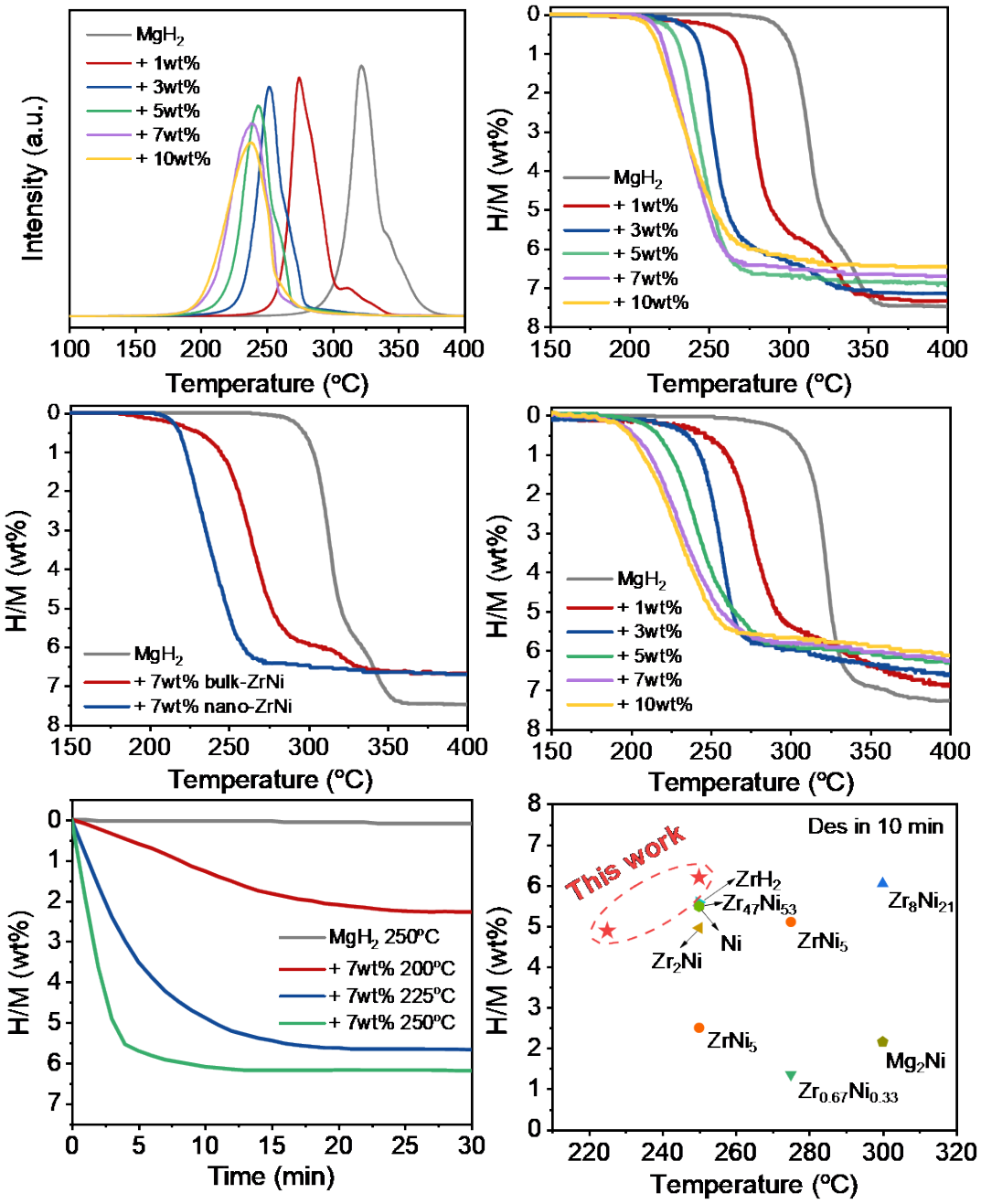

Figure 2. TPD curves (a), first-cycle volumetric release curves of MgH_2 + *x* wt.% nano-ZrNi samples (b), and comparison of MgH_2, MgH_2 + 7 wt.% bulk-ZrNi and nano-ZrNi samples (c). Second-cycle volumetric release curves of the MgH_2 + *x* wt.% nano-ZrNi samples (d). Isothermal dehydrogenation curves (e). Comparison of hydrogen desorption capacity in the first 10 min between our nano-ZrNi-containing MgH_2 and the reported samples (f).

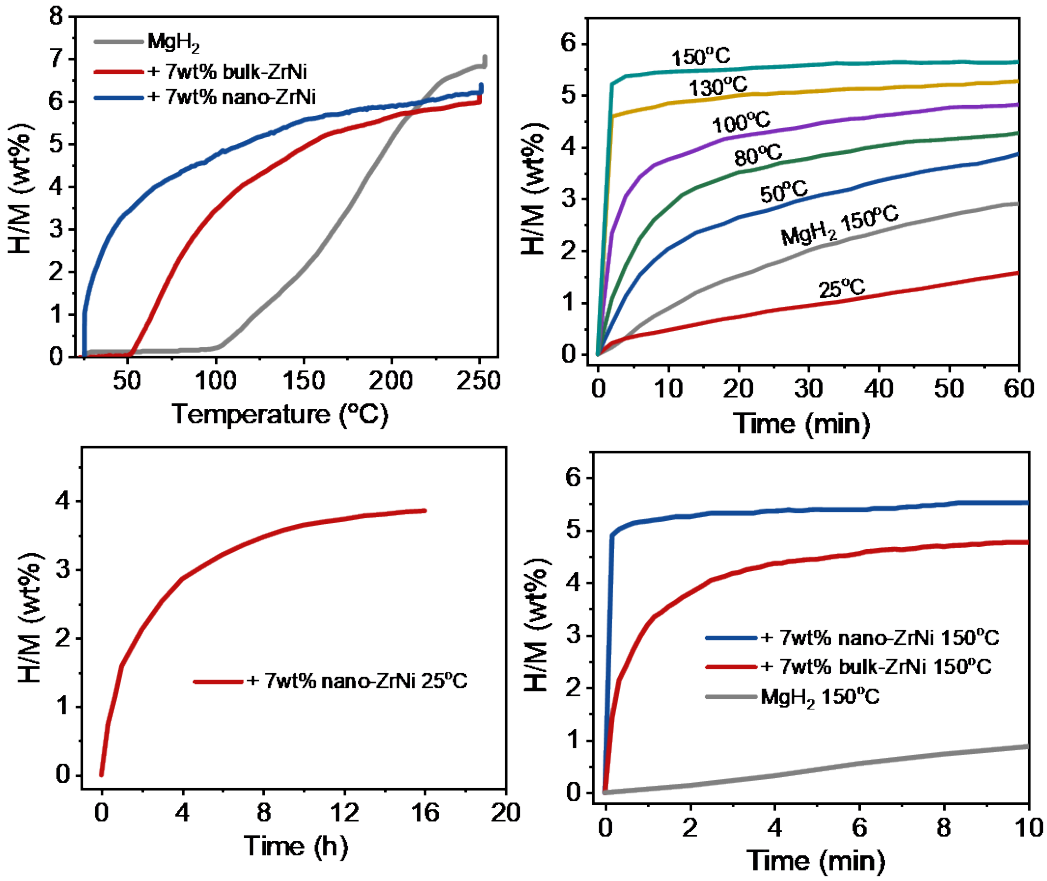

Figure 3. Temperature-dependent hydrogenation curves (a). Isothermal hydrogenation curves of (b) MgH_2 and MgH_2 + 7 wt.% nano-ZrNi samples at various temperatures and (c) MgH_2 +7 wt.% nano-ZrNi at 25 ºC. Comparison of isothermal hydrogenation curves at 150 ºC (d).

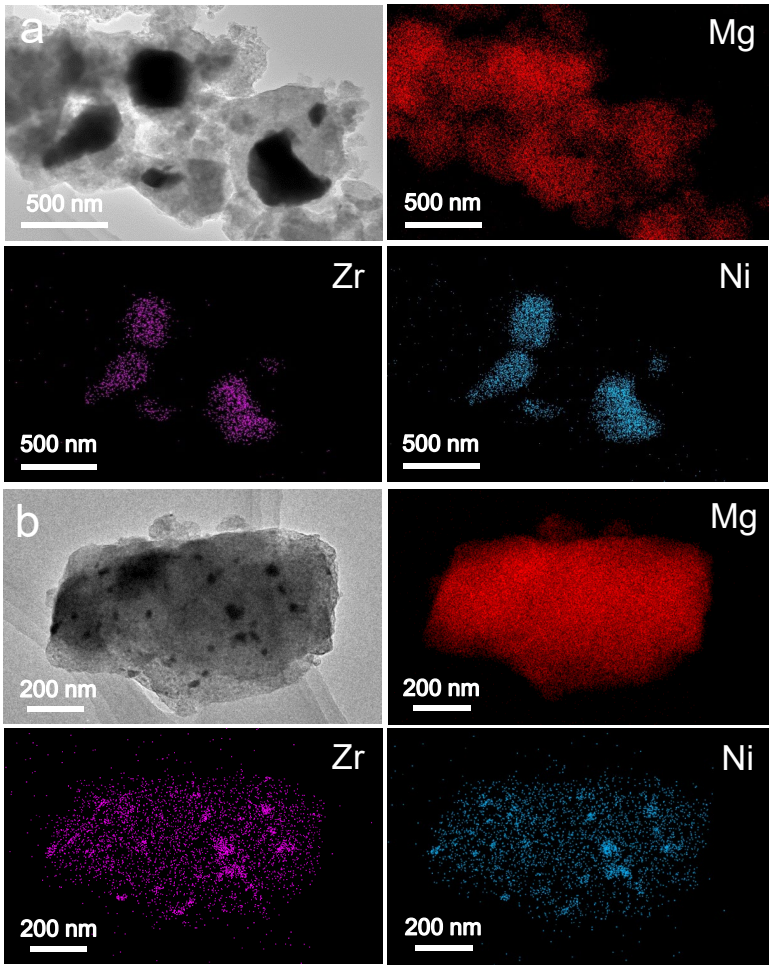

Figure 4. TEM images and corresponding EDS mappings of Mg, Zr and Ni for MgH_2 milled with bulk-ZrNi (a) and nano-ZrNi (b).

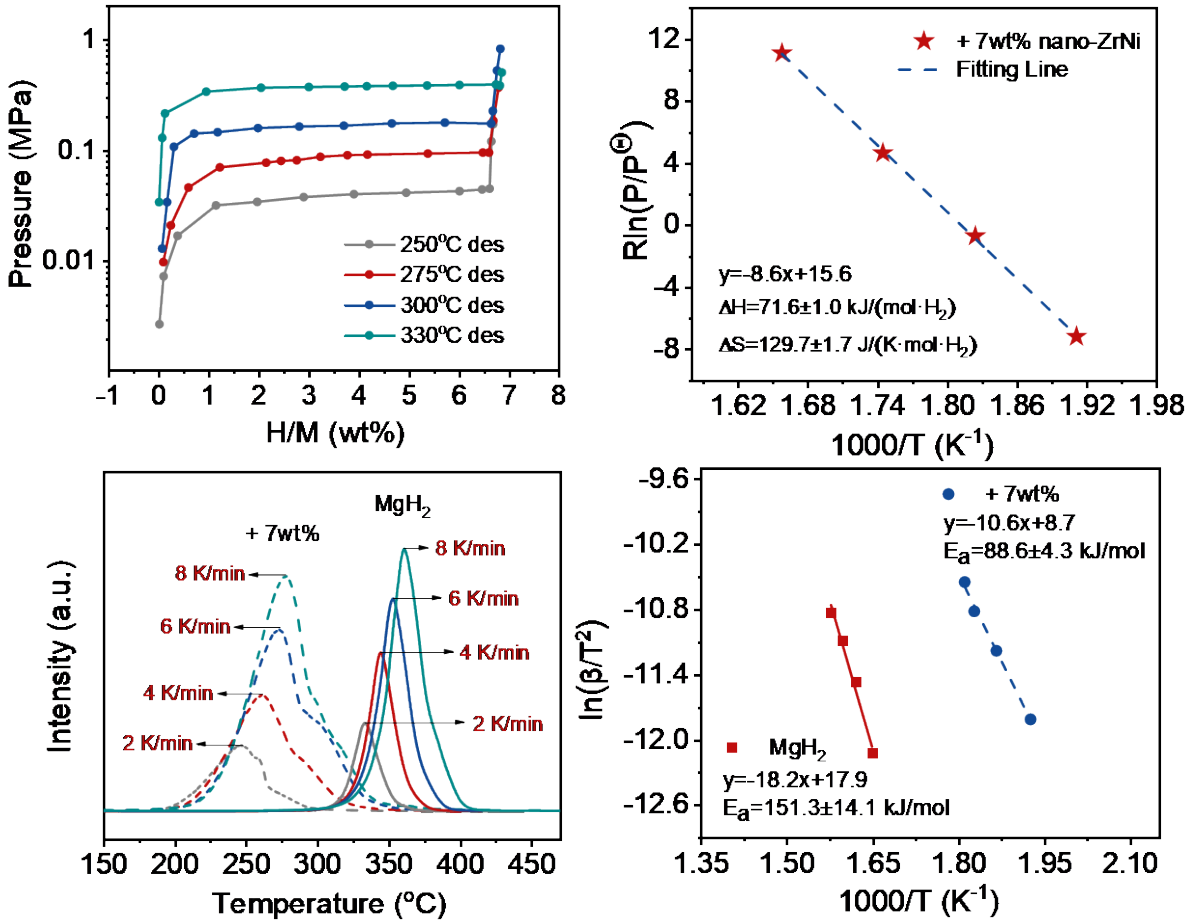

Figure 5. Dehydrogenation PCI curves (a) and van't Hoff plots (b) of MgH_2 + 7 wt.% nano-ZrNi samples. TPD curves (c) and Kissinger's plots (d) of MgH_2 and MgH_2 + 7 wt.% nano-ZrNi samples.

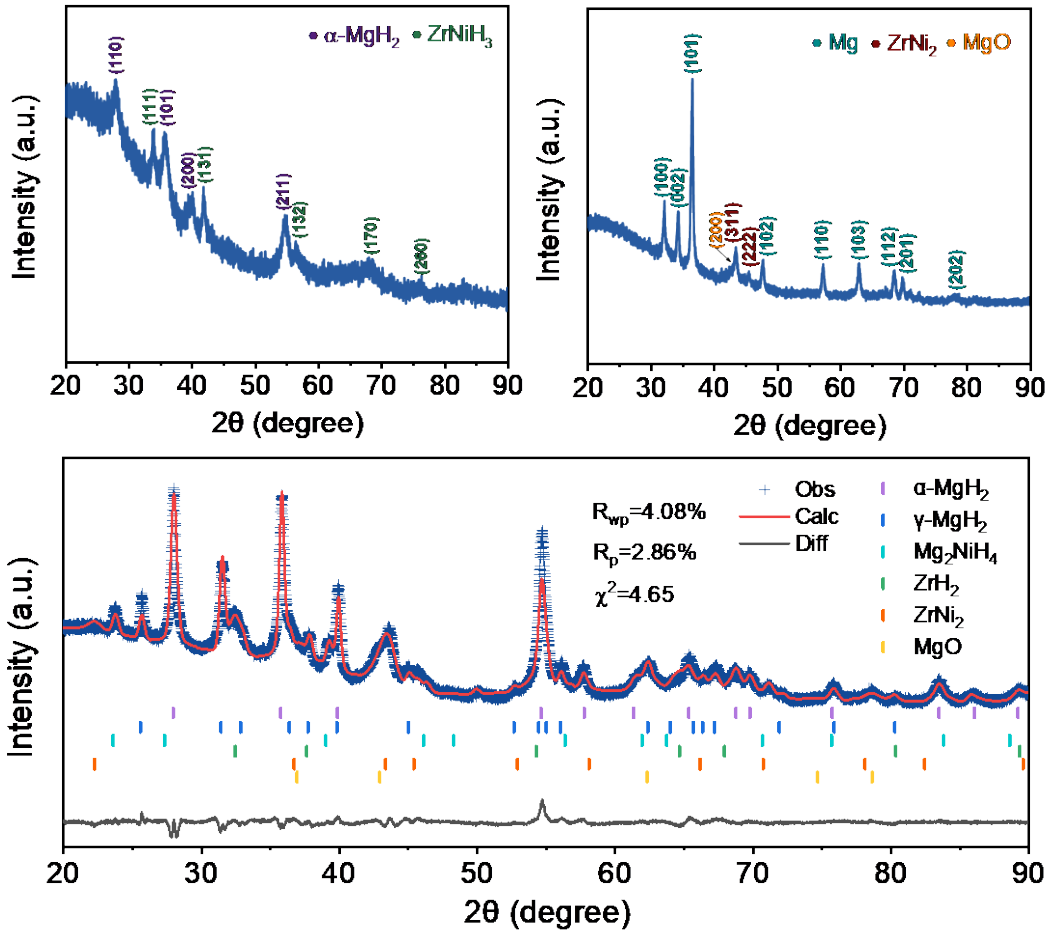

Figure 6. XRD patterns of MgH_2 + 7 wt.% nano-ZrNi sample after ball milling (a), dehydrogenation (b) and rehydrogenation (c). Rietveld refinement was carried out on the XRD pattern (c).

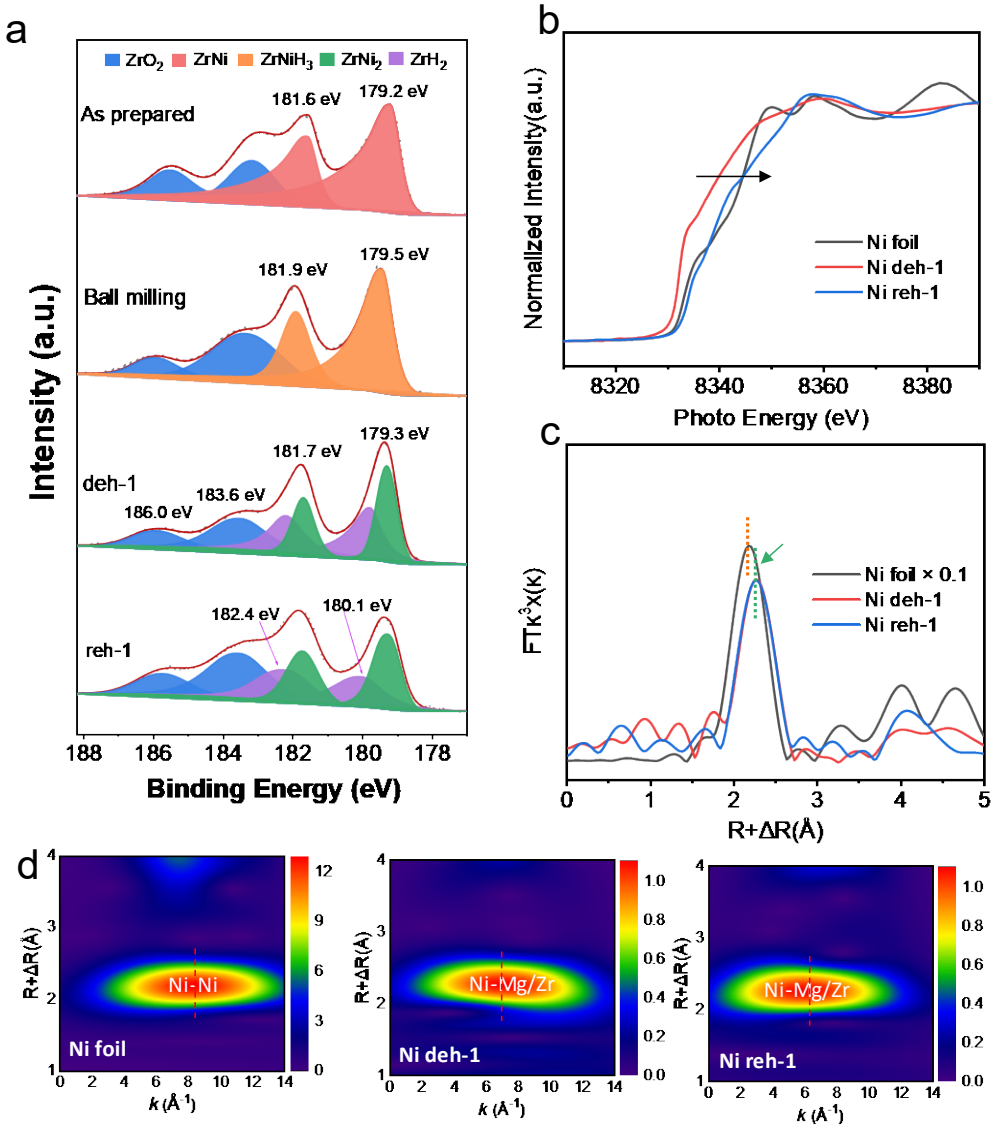

Figure 7. High resolution XPS spectra (a) of Zr 3d in MgH_2 + 7 wt.% nano-ZrNi at different stages. XANES spectra (b) and Fourier transforms (FT) of k^3-weigted EXAFS spectra (c) of Ni foil, Ni deh-1 (after 1st dehydrogenation) and Ni reh-1 (after 1st rehydrogenation) at the Ni K edge. Wavelet transforms (WT) (d) for the k^3-weighted EXAFS signals of different samples.

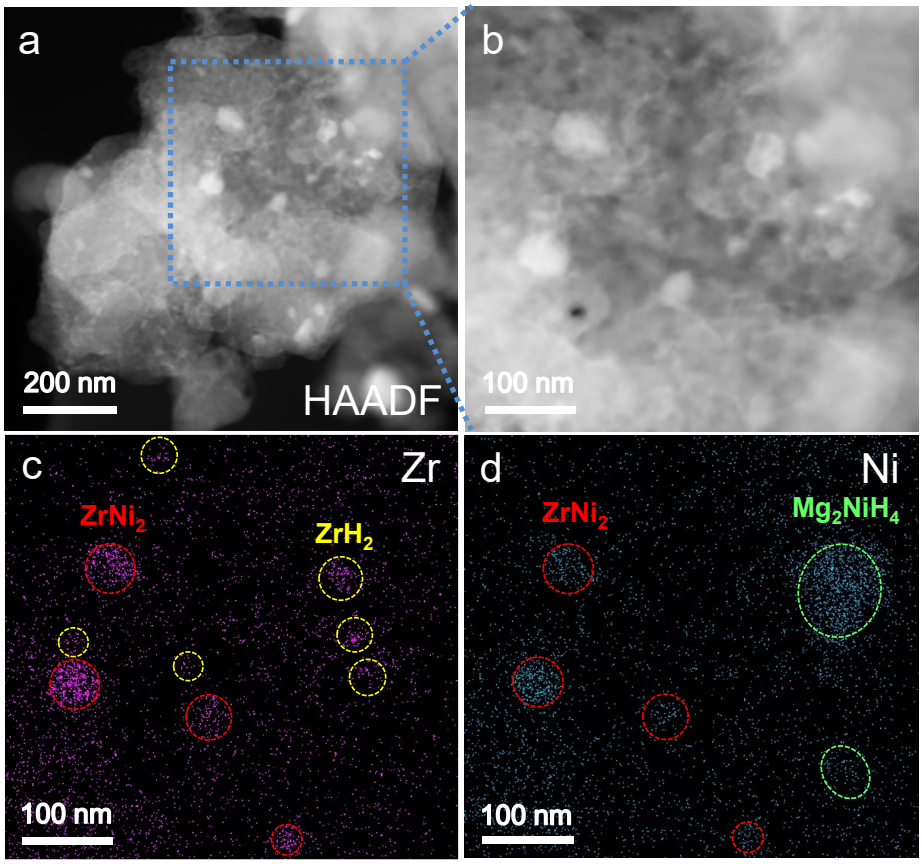

Figure 8. HAADF images of rehydrogenated MgH_2 with 7 wt.% nano-ZrNi (a, b) and corresponding EDS mapping results (c, d). The compounds marked in (c) and (d) were speculated together with the XRD results.

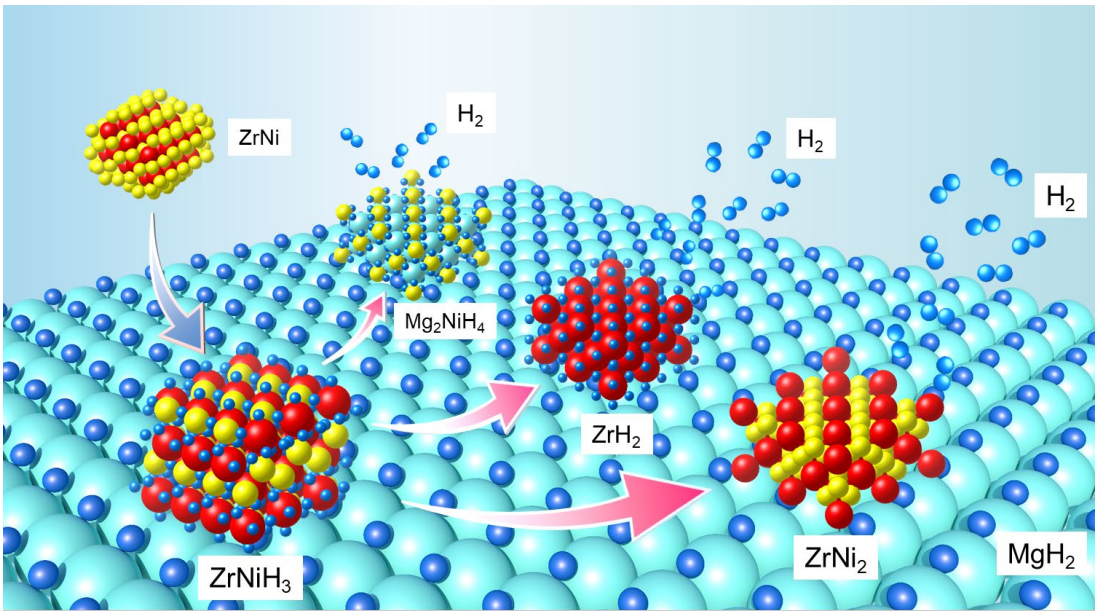

Figure 9. Schematic illustration of the *in-situ* transformation of ZrNi upon ball milling and de-/hydrogenation for hydrogen storage in nano-ZrNi-containing MgH_2.

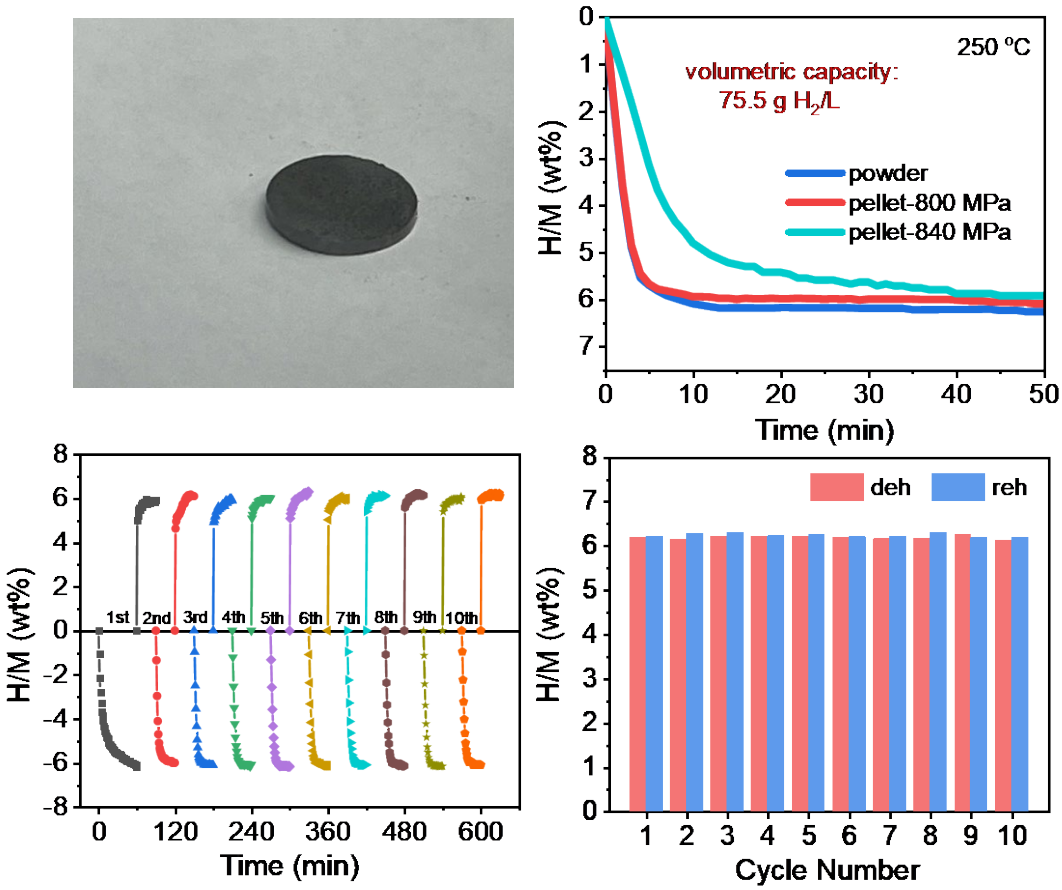

Figure 10. A digital image of the MgH_2 + 7 wt.% nano-ZrNi pellet fabricated under 800 MPa (a), isothermal dehydrogenation curves of the samples in powder form and cold-pressed pellets (b). Isothermal reversible hydrogen absorption and desorption cycling profiles at 250 °C (c) and the cycling capacity (d) of MgH_2 + 7 wt.% nano-ZrNi powder sample.